Inkjet-printed freeform gradient refractive index Alvarez-Lohmann optics for vision correction in respiratory masks

George M. Williams* **and John Paul Harmon**
NanoVox LLC, Beaverton, Oregon, United States

Abstract. Inkjet-print additive manufactured freeform gradient refractive index representations of an Alvarez-Lohmann lens were developed and optimized for use in vision-correction inserts for respiratory masks. A series of planar 30-mm by 20-mm Alvarez-Lohmann lens pair were printed and characterized. Select lens pairs were mounted with printed mechanical lens mounts and translation guides optimized for vision correction. Metrology showed accurate reproduction of the cubic refractive phase functions. Tests matching simulated performance showed a large diopter adjustment over a large eyebox and a wide gaze angle. The printed optics were environmentally tested and then mounted in a respiratory mask and demonstrated with glove-accessible control electronics. The performance demonstrates the benefits of using printed three-dimensional freeform gradient index optics for implementing complex refractive optical functions for challenging applications including artificial and virtual reality systems. [DOI: 10.1117/1.OE.62.3.033103]

Keywords: Alvarez lens; freeform; gradient index optics; gradient index; additive manufacturing; achromatic.

Paper 20221225G received Oct. 19, 2022; accepted for publication Feb. 6, 2023; published online Mar. 14, 2023.

1 Introduction

Freeforms are optical shapes or optical surfaces that are designed with little to no symmetry. The added degrees of freedom afforded by freeforms makes them particularly useful for implementing non-radially symmetric phase plates or for use in off-axis optical systems in which axial symmetry is broken.[1–3] Interest in freeform optics has been particularly driven by potential applications in near eye displays as well as compact optical systems for medical, military, and mobile imaging[3] and illumination[4] devices where there are stringent constraints on size and weight.

Cubic-phase optical elements are freeforms of particular interest. Cubic lenses have been shown to exhibit increased depth of focus.[5] A variant of cubic-phase optics of particular interest is a focus-correcting lens called the Alvarez or Lohmann (Alvarez-Lohmann) type lens.[6–9] Despite a simple operating principle, for some time since its invention, the Alvarez-Lohmann lenses remained impractical due to the aberrated optical performance of practically manufactured elements;[10,11] the manufacture and metrology of transmissive cubic surfaces with the necessary precision remains a time-consuming and often expensive process.[12,13] Moreover, as existing refractive freeforms are made using homogeneous materials, complex chromatic aberrations result from the dispersion introduced at their shaped surfaces. Freeform gradient-index (GRIN) optics offer a method of addressing these limitations and provide a practical method for fabricating improved performance Alvarez-Lohmann lenses optimizing for specific applications.

GRIN has been the subject of considerable research.[2,14–19] It has been shown that GRIN offers added degrees of freedom in the form of dimensionally varying index gradients,[1,2,20–25] that may be used to reduce the size and weight of optical systems.[1,24], However, limited by available fabrication processes, GRIN lens geometries have historically been limited to modest radially symmetric index gradient profiles, their size limited do manufacturing constraints, and their

*Address all correspondence to George M. Williams, georgew@nano-vox.com

dispersion characteristics limited by process compatible materials.[26–29] Recent advancements in the manufacturing of GRIN media now make possible refractive index distributions that may vary arbitrarily in up to three spatial dimensions, $n(x, y, z)$.[15,30–34]

Additive manufacturing of optics has been another vibrant area of research.[35–38] An attribute of additive manufacturing is that designs can be readily fabricated, on demand, directly from software design tools, eliminating the cost and lead times associated with manufacturing conventional freeform optics. It has recently been demonstrated that drop-on-demand inkjet print additive manufacturing can be used to create volumetric index gradients within an optical element.[21,30,30–32] In addition to enabling fabrication of radially symmetric spheric GRIN elements, using inkjet print manufacturing it is possible to fabricate complex radially symmetric aspheric index gradients, as well as three-dimensional (3D) aspheric index gradients, wherein high-order gradient profiles vary axially as function of their position on the optical axis.[23,24,24] Inkjet print manufacturing is also particularly well suited for manufacturing freeform index gradients.[20,21,30,31]

Freeform optics have, to date, almost exclusively referred to freeform surfaces; however, freeform GRIN optics offer an alternative method of transforming optical phase.[4] In plano-plano freeform GRIN phase plates, the refractive index gradient controls optical path differences (OPD) rather than the summation of figure thicknesses, as is the case for shaped homogeneous index freeforms.

While there are similarities between freeform GRIN and freeform surfaces, a distinct benefit of freeform GRIN is that plane parallel freeform GRIN has degrees of freedom in three dimensions, $n(x, y, z)$, whereas freeform surfaces have degrees of freedom in two dimensions, $z(x, y)$. With 3D freeform GRIN it is possible to implement arbitrary volumetric gradient profiles in which there are no axis of symmetry. The ability to create polynomial terms with longitudinal (i.e., z direction) variations in the GRIN profiles provides extra degrees of freedom, not available with surface figured freeforms, which can be used to correct for axis deviation, reduce aberrations, accommodate non-paraxial rays, and otherwise improve the performance of Alvarez-Lohmann lenses.

Significantly, the ability to engineer multiple nanocomposite optical materials using multi-constituent blends, and to then mix the multiple multiple-constituent optical feedstocks when print composing substrates, makes it possible to independently specify the index gradient and the dispersion of additively manufactured GRIN optical materials, allowing for fabrication of achromatic singlet lenses and achromatic freeform refractive optics.[30]

Several of the degrees of freedom afforded by the inkjet print additive manufacture of freeform GRIN lenses are demonstrated in the optimization, fabrication, and metrology of planar Alvarez-Lohmann lenses demonstrated and environmentally tested for used in accommodating vision in respiratory masks.

2 Corrective Lens Accommodation in Gas Masks

Full-face respirator masks protect workers against all sorts of hazardous and harmful elements including gases, dust, smoke, vapors, sprays and other toxins. From the inherent nature of their use, respirator masks are designed to fit snugly to the face of the wearer. However, while many tactical masks are optically correct across the wide field of view and are generally compatible with night vision googles and weapon sights, it is very difficult for a person wearing prescription or special glasses to adjust the mask for a proper fit without compromise to visual performance. To adapt respiratory masks for corrected vision, clip inserts containing the prescription lenses are often provisioned. These inserts fit inside the face piece, directly behind the mask window, and must be individually aligned by the user.

While the inserts must be mounted to the mask, for good visibility the prescription lenses should be close to the eyes of the wearer. Unfortunately, to prevent fogging, the windows in gas masks are frequently at a considerably greater distance from the wearer's eyes than the optimum distance for the prescription lenses. Another limitation is that clear vision is achieved only over a limited range of gaze directions, since the eye must be directed through the restricted area of the lens element implementing the corrective power. When wide-field-of-view gas mask windows

are employed, which cut across normal lines of vision at oblique angles, there is great difficulty in mounting the prescription lenses within the mask's facepiece in correct optical relation to the wearer's eyes.

The problem of vision accommodation isn't limited to respiratory masks. Similar challenges are faced by designers of artificial (AR) and virtual reality (VF) systems.

3 Alvarez-Lohmann Type Lenses

The Alvarez-Lohmann class of lenses offers a unique method of performing positive and negative diopter adjustments necessary for vision accommodation in respirator masks. The Alvarez-Lohmann is a composite lens that consists of two spatially separate variable phase plate elements that combined to make an effective lens. A schematic of a common implementation of an Alvarez-Lohmann is shown in Fig. 1(a). In its most common implementation, both lens components are plano-freeform elements with the surface geometries described by a cubic polynomial equation;[10] the first element features the negative function of the second $[f_1(x, y) = -f_2(x, y)]$. With translation between the upper and lower parts of the device, the surface functions are designed to produce quadratic wavefront changes.

In a traditional Alvarez-Lohmann lens, the two variable phase plates are aligned along the optical axis with the cubic surfaces inverted with respect to each other. When laterally aligned, the effective cumulative thickness introduces a phase delay proportional to the combined thickness of the shaped elements.[39] The structure is designed such that at one value of lateral shift, $\delta = \delta_0$, between the two parts, the device acts as a neutral optical element which does not change the wavefront of a propagating plane owing to the cancellation of the cumulative phase delays introduced by the surface profiles of one element by those of other element. Thus, the system has an infinite focal length.

The optical power of the device changes proportionally with the lateral shift, δ. By performing a transverse shift of the surfaces relative to one another there is no longer perfect cancellation of the variable phase delays of the two elements. In this case, the component can be described by a phase function distribution corresponding to a simple delay on the incident illuminating wavefront that is proportional to the effective thickness of the composite surfaces. The differential of the two cubic profiles results in a composite surface with a spherical thickness variation that induces a quadratic variation in the wavefront, such that depending on the direction of the shift, the composite thickness is equivalent to a converging or diverging lens of a certain focal length.[6,7,10]

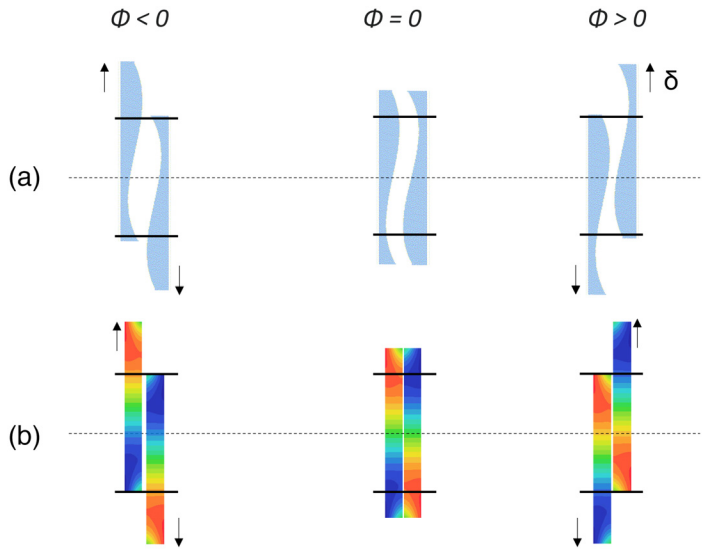

Fig. 1 Alvarez-Lohmann lenses implemented using (a) plano-freeform surfaced homogeneous index materials and (b) plano-plano freeform GRIN.

Alvarez,[6,7] and similarly Lohmann,[8] used this approach to generate varifocal lenses. The difference between Alvarez and Lohmann lens functions is the shape of the cubic surface; the relation between the Alvarez and the Lohmann descriptions is a 45 deg rotation and a scale factor of $\sqrt{2}$. In these designs, each lens has a cubic-type surface profile, which may be represented as

$$z_1(x,y) = A(x^3/3 + xy^2) + Fx + E$$
$$z_2(x,y) = -A(x^3/3 + xy^2) - Fx + E, \tag{1}$$

where x and y are in-plane transverse coordinates normal to z, representing position, and A, D, and E are design variables.

While their values can highly influence wavefront error (WFE), both the F and E coefficients have no direct effect on the focal length. The coefficient E is a constant representing the lens element thickness at δ_0; it can be adjusted to reduce overall lens thickness.[40] While a finite gap is necessary to prevent collisions between the surfaces as they are shifted, assuming that there is no gap between the elements, when aligned at δ_0, the combined thickness of the two-element system is $z = z_1 + z_2 = 2E$, an equivalent of a parallel plate. Meanwhile, the coefficient F defines the tilt term of the freeform surface that affects the slope of the prism along the 'x' direction of the cubic profile; it may be used as a compensating term to reduce the effects on sag that result from increasing the coefficient A. The coefficient A is the area scale that represents the rate of lens power variation with lens movement in the x direction.

Working within the thin lens and paraxial approximations, one can vary the focal length of the composite pair by transversely shifting the plates relative to one another. The optical power varies linearly with δ, and both positive and negative power can be obtained by altering the direction of shear (i.e., the sign of δ). When the first element moves a displacement δ and the second moves $-\delta$ along the x direction, the combined thickness, z, has a parabolic term $-2A\delta(x^2 + y^2)$. The parabolic term is equivalent to a standard axially symmetric constant curvature term. For a determined lateral displacement range, the value of A affects the sag and curvature of the object conjugate plates. The effective sag of the composite surfaced pair gives rise to a focal point. In order to relate the spherical profile to focal length, a first-order paraxial approximation is assumed. From the sag equation of a surface, the radius of curvature, r, is given as

$$R = 4r\delta. \tag{2}$$

The effective focal length, f, of the combination, can then be calculated as

$$f = [4A\delta(n-1)]^{-1}, \tag{3}$$

where n is the refractive index of the lens material.[41] The refractive index contributes to the optical path difference, and this generally forces both components to be the same material if they are identical cubic surfaces. However, if both the coefficient A and n are changed proportionally, it is possible to maintain purely quadratic phase variations.

The performance limitations of prior Alvarez-Lohmann lens implementations stem from the deviation of practically manufactured lenses from their thin lens approximations, which is exacerbated by the air gap between the pair. A thin lens approximation allows the Alvarez-Lohmann lens to be represented by two cubic functions superimposed on top of one another, such that the coordinates at which the ray of light exits the first element and the coordinates at which it intersects the second element are the same. However, if the phase plates have a finite thickness and are separated—as is the case with homogeneous index surfaces—there can be a significant difference between the ray coordinates from theoretical, which often causes Alvarez-Lohmann lens implementations to deviate significantly from their ideal performance.[10,11,14]

Obtaining a wide fixed gaze angle, θ_{gaze}, over a large diopter range, D, within the lens size constraints and displacement limitations, δ_{max}, requires optimizing the coefficients of Eq. (1) such that minimum WFE is obtained across the clear aperture of the lens pair, which defines the eyebox shown in Fig. 2. To obtain a large range of lens powers with minimal lateral translation, the value of A needs to be large which, in turn, increases the lens sag. This causes the lenses to be increasingly thick away from the optical center.

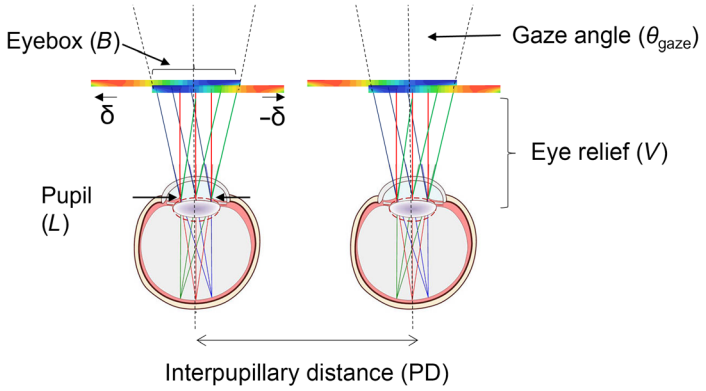

Fig. 2 Diagram, showing design variables of VCIs for respiratory masks showing application specific design variables.

Obtaining a large optical power adjustment range in a compact configuration is also challenging. The change in optical power is proportional to the product of A and the lateral displacement, δ; so, for a compact implementation, δ_{max} must be made small, which requires that A be large. However, increasing the value of A increases curvature, which in turn increases the sag and causes larger amounts of aberrations from the combined elements. Because the elements are non-rotationally symmetric freeforms, aberrations specific to off-axis propagation, including coma and astigmatism may also degrade performance.[42]

Higher-order surface terms may be used to partially compensate for these aberrations;[11,43,44] however, realizing precise high-order freeform surfaces is constrained by existing process limitations, and the correction is difficult to maintain throughout the power range. Moreover, as prior Alvarez-Lohmann lenses have been realized using homogeneous optical media (e.g., glass or plastics), chromatic aberrations present a genuine limitation. Combined with the non-superposition of the dual optical functions resulting from lens thickness, optical axis dislocation, and non-paraxial behavior of gaze angles, practical Alvarez-Lohmann lens implementations deviate from their ideals.[10,44]

4 Printed Freeform Gradient Refractive Index Optics

To address the needs of freeform refractive optic systems, NanoVox has developed a custom additive manufacturing technology platform, called "variable index of refractive gradient optics" that uses inkjet printhead deposition of specific compositions of optical nanocomposite feedstock.[30,31]

The properties of the printable primary "optical ink" feedstocks play an important role in inkjet constructed optical elements. The nanocomposite optical feedstocks are formulated by embedding one, or more, non-scattering organic or ceramic nanoparticles in one, or more, low-viscosity optical-grade photocurable monomers. Each nanoparticle is small (e.g., $< \sim 10$ nm, less than 1/30th the wavelength of light passing through the optic) and is chemically coated to eliminate agglomeration, such that Rayleigh and Mie scattering are insignificant.[30] The optical inks are formulated with the rheological properties necessary for reliable inkjet printhead deposition.[45–47]

At minimum, using inkjet print fabrication, two optical inks are necessary to create a GRIN element, a "high index" optical ink, n_{high}, and a "low index" optical ink, n_{low}. The difference in the index values of the two primary inks is the refractive index contrast, Δn. A unique feature of multi-constituent nanocomposite optical inks is that it is possible to precisely tailored the refractive index spectra of the optical inks relative to one another, to control primary and secondary color. The refractive index spectral properties of the primary optical inks are a linear function of the volume fraction of the inks' constituent properties[48–50] The dispersion of homogeneous materials over the "d; F; C" spectrum is commonly characterized by the Abbe number, ν, and partial dispersion, P, as

$$\nu = (n_d - 1)/N_F - n_C), \tag{4}$$

$$P_{d,F} = (n_F - n_d)/(n_F - n_C). \tag{5}$$

For homogeneous materials with normal dispersion, ν is always positive and the value of P is around 0.7 and is bounded between zero and one.[30] The partial dispersion values of optical materials strongly trend linearly with their dispersion values.[51,52]

For GRIN optics, the GRIN Abbe number (ν_{GRIN}) and partial dispersion ($P_{d,F\,\mathrm{GRIN}}$) are defined as[53]

$$\nu_{\mathrm{GRIN}} = (\Delta n_d)/\Delta n_F - \Delta n_C), \tag{6}$$

$$P_{d,F\_\mathrm{GRIN}} = (\Delta n_F - \Delta n_d)/(\Delta n_F - \Delta n_C) \tag{7}$$

so that their values are no longer constrained. Defined by the difference in the refractive index spectra of the high and low index primary optical inks used to print the gradients, the index gradients can have positive, zero, or negative ν_{GRIN} values, and when more than three constituents are used to synthesize the feedstock, the dispersion can be defined independently from the index gradient.[30,49,50,54]

Independent control of dispersion relative to the index gradient allows for achromatic singlet GRIN lenses to be fabricated. For example, even for a binary primary optical ink pair, when the slope of the high-index optical inks, $n_F(\mathrm{high}) - n_C(\mathrm{high})$, is matched to the slope of the low-index optical ink, $n_F(\mathrm{low}) - n_C(\mathrm{low})$, such that $\Delta n_F = \Delta n_c$, the GRIN lens is achromatic.[23,30,55,56] Moreover, by introducing sufficient additional constituents into the feedstock composition, it is possible to relax the dependence of the P_{GRIN} values relative to the V_{GRIN} values;[30] thus, making possible a wide range of anomalous partial dispersion GRIN materials not available in standard glass or plastic materials.[51,52,54] Achieving dispersion and partial-dispersion values independent of the index gradient is of critical important for freeform refractive optical elements, due to the complexity of dispersion attributable to freeform surfaces and GRIN functions.

Increasing the number of primary optical inks expands the degrees of freedom. The number of primary optical inks that can be printed simultaneously is limited by the number of available printheads. For the simple case of a binary ink set, at least two printheads are required. Constructing each layer of the refractive index gradient requires separate bitmaps for each printhead. For each pass of the printhead over the substrate, the bitmaps define the drop density patterns of each primary optical ink.

Using inkjet print deposition, "print composition" is used to define the intermediate refractive index values of the gradient profiles. With spatial droplet concentrations defined by the bitmaps, local mixing and inter-diffusion of the codeposited primary optical inks, causes the spatial localities to assume refractive index spectra that are the weighted average of their constituents' spectral properties. A simple binary linear composition model[57–59] allows the substrate index value to be approximated at each wavelength as a function of two primary optical inks, $n_{\mathrm{low}}(\lambda)$ and $n_{\mathrm{high}}(\lambda)$, as given in the following equation:

$$\begin{aligned} n(x,y,\lambda) &= C(x,y)_{\mathrm{low}} n_{\mathrm{low}}(\lambda) + C(x,y)_{\mathrm{high}} n_{\mathrm{high}}(\lambda) \\ &= (1 - C(x,y)_{\mathrm{high}}) n_{\mathrm{low}}(\lambda) + C(x,y)_{\mathrm{high}} n_{\mathrm{high}}(\lambda) = n_{\mathrm{low}}(\lambda) + C(x,y)_{\mathrm{high}} \Delta n(\lambda), \end{aligned} \tag{8}$$

where $C(x,y)_{\mathrm{low}}$ and $C(x,y)_{\mathrm{high}}$ are the local volume concentrations of the primary optical inks defined by index n_{low} and index n_{high}, respectively, at location (x,y), and $\Delta n(\lambda) = n_{\mathrm{high}}(\lambda) - n_{\mathrm{low}}(\lambda)$.

In the graphics print industry, halftoning algorithms are used to determine the placement of the optical ink droplets such that the reflective properties of the substrate create grayscale images, using only black droplets.[60] To create refractive GRIN profile bitmaps using optical ink pairs, a comparable process is used. To accommodate three-dimensional refractive index volumes, i.e., $n(x,y,z)$, the halftoning algorithms quantize the refractive index profile designs in three dimensions. The residuals from quantization are distributed to neighboring pixels that

have not yet been processed. This method can also be extended to three-level or multi-level halftoning, so that several primary inks can be printed simultaneously. Printing multiple inks reduces the levels of quantization, allowing for more precise control over GRIN patterns. Simultaneous printing of multiple inks also provides degrees of freedom for controlling dispersion and secondary color.

The stack of print maps, one for each printhead each layer, are uploaded to the printer when fabricating the optic. Using industrial printers, the drop placement of the optical inks can be controlled to better than one micron precision, but after inter-diffusion of the concentrations of optical inks and polymerization, it is possible to fabricate complex subwavelength smooth gradient profiles that precisely match the design intent.

Planar freeform-GRIN elements can be printed with better than $\lambda_{632\ \mathrm{nm}}/14$ flat surfaces, without postprocessing.[25,30,61] Due to the benefits of the inter-dispersed ceramic nanoparticles that are tightly crosslinked within the polymer matrix, the nanocomposite optical materials are sufficiently strong and hard that, using industry standard processes, the surfaces may be polished or shaped to high precision industry standards.[31] The nanocomposite materials are also non-hydroscopic and have lower temperature sensitivity than plastic materials.

5 Gradient Index Alvarez-Lohmann Varifocal Lens Optimization

Inkjet printing of nanocomposite GRIN materials allows for performance optimization of Alvarez-Lohmann type lenses not readily available using surface shaped homogeneous materials. In a plano-plano freeform GRIN Alvarez-Lohmann lens [e.g. see Fig 1(b)], optical power is generated similarly to that of surface-figured homogeneous index elements; however, rather than sum the thicknesses attributable to the surface shapes of each element, the OPD across the GRIN phase plates is determined by Δn and the element thickness, t.

Assuming no variation of the refractive index perpendicular to the optical axis (i.e., z- axis), the generally Alvarez-Lohmann cubic phase profiles may be represented for GRIN implementations as

$$\begin{aligned} n_1(x,y) &= n_{00} + k(x^3/3 + xy^2 + Rx + E) \\ n_2(x,y) &= n_{00} - k(x^3/3 + xy^2 - Rx + E), \end{aligned} \tag{9}$$

where $n_i(x,y)$ is the refractive index at point x,y on the lens, n_{00} is the base index (value of the lowest index optical ink), the index profile coefficient k is a scaling factor that describes the magnitude of the refractive index term, the coefficient R is a field constant that describes the tilt term, and E is a scalar constant, which here for simplicity we set to zero. It is assumed there are no axial (z-direction) refractive index gradients.

The similarity between Eq. (9) and Eq. (1) is apparent. The index profile coefficient k of Eq. (9) functions equivalent to coefficient A of Eq. (1) used to describe the magnitude of lens power variation for surfaced Alvarez-Lohmann lenses. The coefficient R of Eq. (9), when scaled by the coefficient k (i.e., R/k) is functionally equivalent to coefficient F of Eq. (1), which governs the amount the polynomial functions are tilted.

For a thin Alvarez-Lohmann component, the variation in OPD within the clear aperture of a single thin plano-plano lens plate, is given as

$$\mathrm{OPD}(x,y) = t[n(x,y) - n_{00}], \tag{10}$$

where n_{00} is the base refractive index value at which point OPD $= 0$. The OPD of the combined elements is obtained by summing the index maps of Eq. (10), calculated with x varied $+/-\delta$ relative to one another other, with a combined thickness of $2t$.

The eye is a compound optical system, and an eye-lens-object optical system is set according to wearer's visual performance and the characteristic of the lens assembly, defined by dioptric power, astigmatism, and visual axis.[62] For use in vision corrective optics, we model the optical power of the Alvarez-Lohmann lens as a radial lens, fitting within the eyebox, with a focal length, f_{GRIN}

$$f_{\mathrm{GRIN}} = r^2/(2t\Delta n), \tag{11}$$

where Δn is the maximum index change across the eyebox, r is half the width of the eyebox, t is the thickness of the lens. The focal length is inversely proportional to diopters according to the relation $D = 1000/f_{\mathrm{GRIN}}$; thus

$$D = (2000t\Delta n)/r^2. \tag{12}$$

There are different combinations of t and Δn that grant the same power variation and increasing either t or Δn enables larger values of the coefficient k which enables high optical power to be achieved.[63] However, Δn is practically limited by the properties of the available optical feedstock. With materials optimized for inkjet printing, which are constrained by the printhead-compatible rheological properties of the optical inks, Δn is typically between 0.06 and 0.12 in the visible wavelength range. For some industrial printheads, Δn values larger than 0.28 are possible.

Figure 2 shows a schematic of the optical layout of the Alvarez-Lohmann lens system used for vision accommodation. The gaze angle (θ_{gaze},) for each lens pair may then be modeled as:

$$\theta_{\mathrm{gaze}} = \tan^{-1}[(B - L)/(2V)], \tag{13}$$

where V (mm) is the eye relief, defined as the vertex distance from the cornea to the back of the lens, which we assume is mounted near the face of the mask, L (mm) is the pupil size, and B (mm) is the eyebox size. The tradeoff constraints of eyebox size, gaze angle, θ_{gaze}, and the eye relief, V, are apparent.

A design trade study was conducted to optimize a GRIN Alvarez-Lohmann lens for vision correction inserts (VCIs) used in respiratory masks. Based on the application requirements, the eyebox size was specified as $B > 10$ mm. The normal pupil size (P) in adults varies from 2 to 4 mm in diameter in bright light to 4 to 8 mm in the dark and was nominally assumed 3 mm for this study. Because the inserts must be mounted between the eyeglasses and the mask surface, the eye relief (V) of the corrective lenses, is constrained by the distance to the mask face. A minimum vertex distance of 7 mm is required to minimize fogging. A horizontal θ_{gaze} of greater than 30 deg was specified. For practical implementation with actuators in a respirator mask, the transverse shift range was limited to $\delta = +/-7.5$ mm.

An extension to the ZEMAX optical design software package, developed by the Naval Research Laboratories (NRL), was used to optimize the design.[16] This extension uses the input data—the index profile $n(x, y, z)$ and gradients of function (dn/dx, dn/dy, dn/dz)—to create generalized, non-radial-index field variations. The ZEMAX optimizer then uses ray tracing to locate a ray at an x, y, z location, and uses the index and gradient slope values at the location to calculate the direction that the ray refracted.

Within the constraints of the application, the Alvarez-Lohmann cubic profiles were optimized by varying the coefficients k and R, which were assumed equal and opposite for each element. To select the ideal scaling factor, k, and field constant, the contributions of the Seidel aberrations and the overall RMS WFE were evaluated at various positions in the eyebox.

A number of different modeled Alvarez-Lohmann designs were fabricated and characterized using digital holographic microscopy (DHM). An example Alvarez-Lohmann lens element, with corresponding wavefront phase delay measurements, is shown in Fig. 3.

The summary of nine different designs selected from the design trade study is shown in Table 1. Designs A and B are implemented with $\Delta n = 0.089$ and differ from each other by the value of coefficient R, which describes the tilt term. The thickness of the elements is minimized when Δn is maximized and the tilt term is optimized. Figure 4 shows the refractive index profile and the optical power achieved as a function of transverse lateral shift for these two designs. Design A was implemented without tilt and as a result was 3.57 times thicker than design B. As shown in Table 1, due to it being thinner, Design B had lower WFE across the eyebox than did design A.

Designs C through G were all designed to achieve the same optical power (+/- 5D) and were configured with $\Delta n = 0.06$. The progression of these lens designs decreased the coefficient k values, which influences the term for refractive index power, and increased the coefficient R values, which influences the term for tilt. The effects of varying the two coefficient values

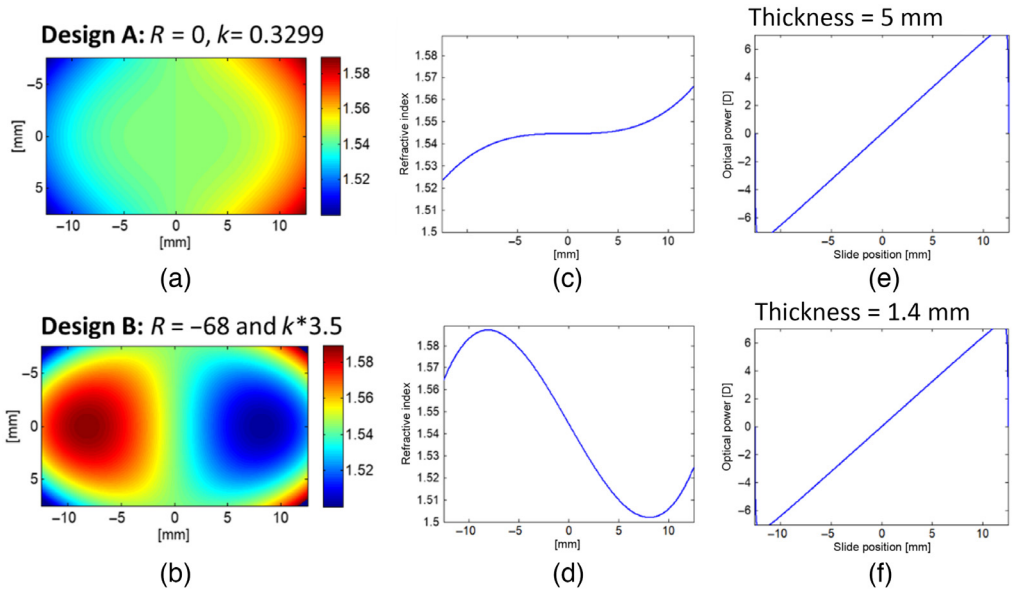

Fig. 3 Designs A and Design B freeform GRIN representations of the optimized Alvarez-Lohmann type lenses, which differ by the tilt term (R), showing the (a) two-dimensional plot of the color represented index profiles; (b) x-axis index profile of refractive through the center of the optic; and (c) optical power achieved with lateral translation of the optic. The thickness of each lens is included.Designs A and Design B freeform GRIN representations of the optimized Alvarez-Lohmann type lenses, which differ by the tilt term (R), showing the (a & b) two-dimensional plot of the color represented index profiles of each design; (c), (d) x-axis index profile of refractive through the center of each design; and (e), (f) optical power achieved with lateral translation of the elements for each design. The thickness of each lens is included.

on the WFE, required lateral shift, width/eyebox ratio, and the element thickness are shown in Table 1. Design C could not achieve sufficient eyebox size. As can be seen in Table 1, the WFE is lowest for Design G, which has the lowest coefficient k value and the largest width/eyebox ratio. This is not surprising, as introduced above, minimizing the rate of optical power generation as

Table 1 Select GRIN Alvarez-Lohmann lens design trade study.

Lens Design	A	B	C	D	E	F	G	H	I
Index rate constant (10^{-4}), k	0.329	1.152	3.33	2.97	1.71	1.71	0.987	3.33	3.41
Field tilt constant, *R*	0	68	25	25	38	38	56	38	38
R/k (10^4)	0.00	59.03	7.51	8.42	22.22	22.22	56.74	7.51	11.14
Optical power (±D)	5	5	5	5	5	5	5	5	9
GRIN Δn	0.089	0.089	0.06	0.06	0.06	0.06	0.06	0.06	0.12
Thickness (z, mm)	5	1.40	0.5	0.84	0.98	1.22	1.26	1.4	1.1
Lateral Shift (Δδ, mm)	7.5	7.5	7.5	5	7.5	6	10	7.5	6
Lens Width (mm)	25	25	20	20	25	25	30	25	25
Eyebox width (mm)	10	10	5	10	10	10	10	11	11
Width/Eyebox Ratio	2.5	2.5	4	2	2.5	2.5	3	2.5	2.5
WFE – eyebox center	0.0044	0.0012	0.0004	0.0011	0.0009	0.0014	0.0008	0.0010	0.0039
WFE – eyebox edge x (left)	0.0202	0.0068	0.0009	0.0067	0.0084	0.0076	0.0049	0.0030	0.0254
WFE – eyebox edge y (top)	0.0405	0.0127	0.0008	0.0065	0.0051	0.0077	0.0049	0.0130	0.0234

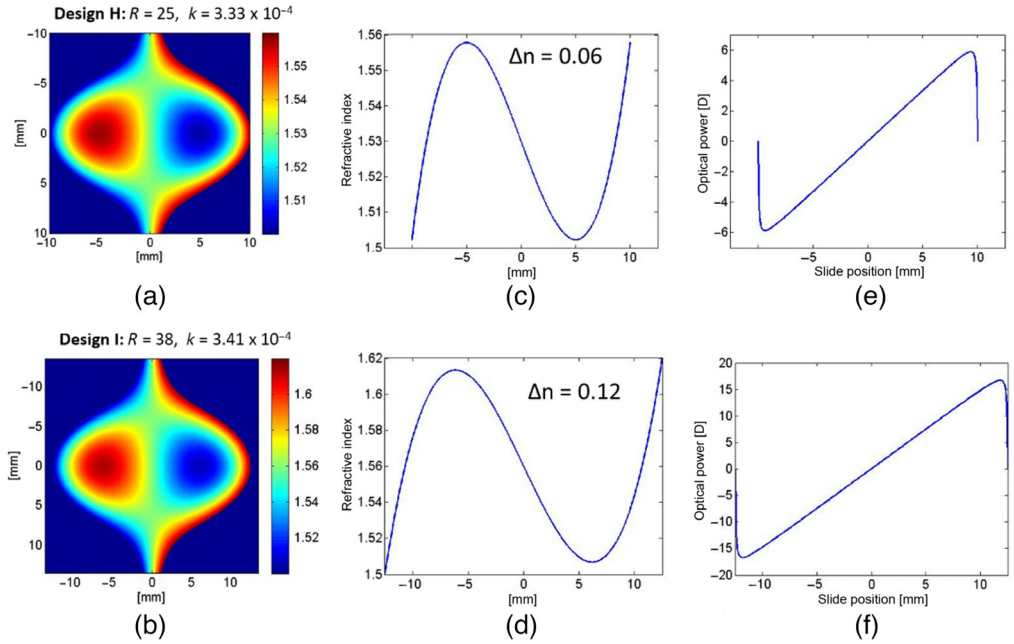

Fig. 4 Design H and Design I freeform GRIN representations of the optimized Alvarez-Lohmann type lenses, characterized by the listed Δn values, showing (a), (b) two-dimensional plot of the color represented index profiles pf each design; (c), (d) the x-axis index profile of refractive through the center of each design; and (e), (f) the optical power achieved with lateral translation of each design. Shown is the thickness of each lens element.

a function or shift is expected to reduce aberrations. The trends show the importance of using the tilt term to minimize Δn and to optimize performance.

Designs E and F were optimized with the same R and k coefficients and differed only in the lens element thickness. By increasing the thickness, a smaller lateral shift was required, but the WFE increased. This is also expected, as increasing thickness from the infinitely thin ideal increases aberrations.

Figure 5 shows the GRIN profiles and the optical power achieved, as a function δ, for Designs H and I. The designs differ primarily on the required Δn value; Design H was implemented with $\Delta n = 0.06$ and Design I was implemented with $\Delta n = 0.12$. As to be expected, a larger Δn value achieves a larger OPD, which allows for design I to achieve an optical power that is twice that of Design H, in a design 22% thinner and with a smaller δ.

Both Δn values are compatible with the print equipment. Nevertheless, Design H was chosen for implementation in the VCI, as the available $\Delta n = 0.06$ ink set met the specification, and

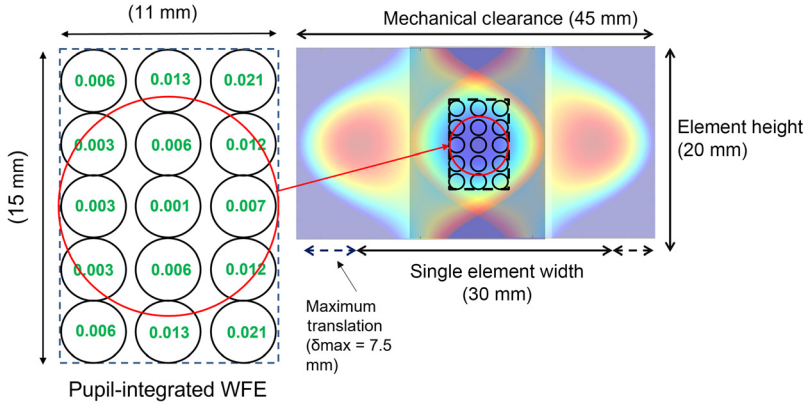

Fig. 5 WFE analysis across eye box of Design H, showing average WFE defined by 3-mm pupils across eyebox. The location of the eyebox within the paired Alvarez-Lohmann lenses is indicated.

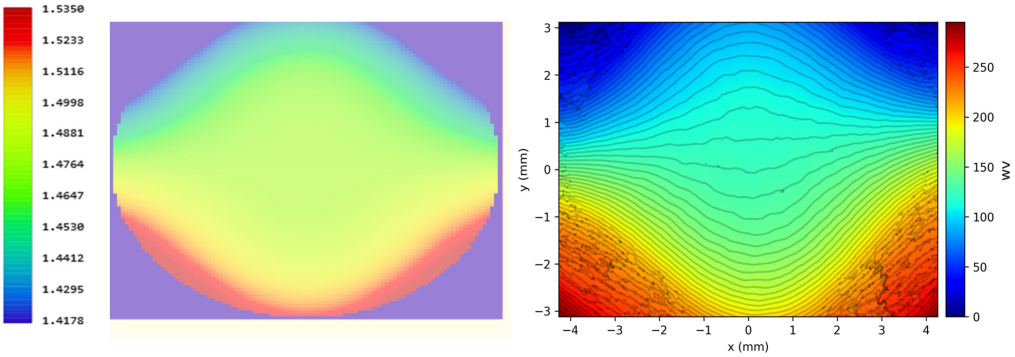

Fig. 6 (a) An example of a high Alvarez-Lohmann GRIN profile map compared to (b) the measured wavefront phase delays from the measured part.

it allows for more control over dispersion. The WFE analysis of the eyebox of Design H is shown in Fig. 6. The WFE was analyzed in 3-mm pupil regions, across the 11-mm eyebox, by comparing the simulated wavefront with a perfect spherical wavefront. The WFE was less than 0.001 waves along the optical axis and the average WFE was less than 0.005 across the entire eyebox. These WFE values are significantly lower than Alvarez-Lohmann lenses previously reported in the literature.[64–66]

6 Inkjet Print Additive Manufacture of Nanocomposite Optics

A series of planar GRIN Alvarez-Lohmann designs from Table 1 were fabricated and tested. The planar GRIN Alvarez-Lohmann lenses were fabricated using a customized graphics ink jet printer (see Fig. 7), which is provisioned with six printheads each with 2,304 nozzles optimized for depositing 21 pL droplets at a 12 kHz rate. The number of printheads determines the number of different inks that can be deposited simultaneously; the number of nozzles and firing rate determines the total rate at which the ink droplets can be deposited simultaneously; and the drop volume dispersed from each nozzle determines the volume rate at which ink is deposited and also defines the granularity of the print masks used to produce the refractive index profiles. Combined, these factors define the mass feedstock deposition rate that governs the build time. When configured with six ink lines, the printheads can dispense up to 12 mL of ink per minute, allowing a single 30-mm × 20-mm × 1.4-mm elements to be fabricated in less than 1 min. The large print swath of each printhead (2.25") and the 48" wide print platform provides room for printing multiple lenses side-by-side, as necessary.

Fig. 7 Customized one-meter format graphics inkjet printer used to produce freeform GRIN optics.

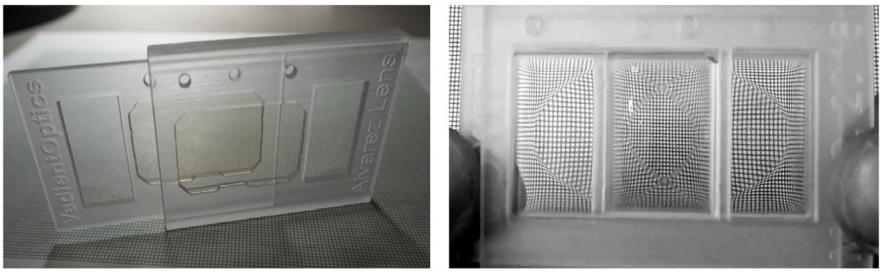

(a) (b)

Fig. 8 Pictures showing two different views of the printed Alvarez-Lohmann lenses, including (a) printed mechanical mounts and guides, and (b) mounts with integrated lens elements.

To create the bitmaps that are communicated to each printheads during fabrication, the designs were first reduced to refractive index value volumes, $n(x, y, z)$. Using the three-dimensional halftoning algorithms that accommodated for the ink diffusion characteristics, the GRIN profiles were translated to bitmap print patterns, which determined the spatial density patterns for the droplets from optical primary ink.[67] As a simple binary ink pair was used to fabricate the lens elements in this efforts, two bitmaps were required: one for the "high index" and one for the "low index" optical ink. As for simplicity, we did not vary the cubic polynomials as a function of the axial coordinate, the same two bitmaps were used to fabricate each layer of the device.

Before printing, the nanocomposite primary optical ink formulations were spectroscopically characterized. We measured the refractive index values for the inks using an Atago Abbe refractometer. The ink compositions were verified using a TA Instruments TGA-2950 Thermo Gravimetric Analyzers with a TA Instruments DSC-2920 differential scanning calorimeters (DSC Q2000). Before printing, the rheological properties (viscosity, surface tension, density, etc.) of the inks were characterized, so that the relative magnitude of the fluid's interfacial, viscous and inertial forces, where within the bounds of drop ejection for the printheads.[45–47]

The Design H Alvarez-Lohmann GRIN lens elements were selected for integration with the prototype VCIs; four of the lenses were integrated with each insert. After fabrication and vitrification, the lenses were laser cut into their final shape. The lens element mounts, mechanical frame of the optical insert, and guides to control the lens pair spacings and lateral shift were also printed using the same printer (see Fig. 8). While we have demonstrated it possible to print the GRIN elements as an integral part of the Alvarez-Lohmann mount, along with the mechanical slide, and self-alignment features, in this effort, the two were printed separately and then mounted together.

7 Vision Correction Insert

Several prototype VCIs were fabricated for integration with the twin filter Avon Protections Systems M50 respirator, which included an Alvarez-Lohmann lens pair for each eye (four Design H plano-plano elements total for each system). The final specifications for the VCI are shown in Table 2.

A major challenge in using Alvarez–Lohmann lenses is designing a mechanical mechanism and attaching it to the frame, in a manner that permits lateral movements without lateral displacement of the elements.[68] Some arrange the lateral movement along the eyelid-cheek (vertical) direction, but others along the nasal-temporal (horizontal) direction.[69,70] In the selected implementation, both of the elements are moved relative to one another. This design enables both the eye relief functionality basic to the design, as well as correction for interpupillary distance under software control. The eyebox can be moved side to side a full ± 7.5 mm in the glasses, accommodating greater than 98% of the population.[71]

The prototype included four glove-accessible buttons that command a microprocessor that allowed the user to power the module, adjust the eye pupil spacing, and change the diopter. At 28 rpm or 0.47 revolutions per second, the lens moves about 2 mm per second. As the optical power is doubled by the relative movement of the elements, the full operating diopter range can

Table 2 Alvarez-Lohmann lens VCI specification.

Parameter	Specification
Optical power range, D (diopters)	+/−5
Minimum eye gaze (h × v), θgaze, degrees	30 × 40
Eye relief, V (mm)	7
Pupil size, P (mm)	2 to 8 (3 nominal)
Minimum eyebox size (h x v), B (mm)	11 × 15
Lateral shift +/− δ (mm)	7.5
Alvarez-Lohmann lens are, l x w (mm)	20 × 30
Alvarez-Lohmann element thickness (mm)	1.4
Time response OD − 5D (sec)	0.2
Accessibility	Glove accessible, four buttons
Operating power	9V battery equivalent
Shock (in mask), g	100
Temperature range (°C)	−45 to 90
Shock and vibration	Mil-STD-810G
Temp/humidity	10°C/+40°C, 0/100%

(a) (b)

Fig. 9 Picture showing VCI in a respiratory mask (a) inserted in Avon50 mask and (b) worn by user (with filter removed).

be reached in about 0.2 s. Four miniature 9-volt-battery-powered haptic-feedback motors, attached to worm gears, were used to drive mating gear racks on the four Alvarez-Lohmann lens elements. The insert was fitted in the Avon M50 respirator and was subjectively evaluated by users (e.g., see Fig. 9) viewing United States Air Force resolution test charts.

8 Characterization

8.1 *Optical Testing and Metrology*

To measure the GRIN disposition of the Alvarez-Lohmann lens pairs, a custom DHM was used to reconstruct the profiles of transmitted optical waveforms. The "as-printed" parts were tested without polishing.

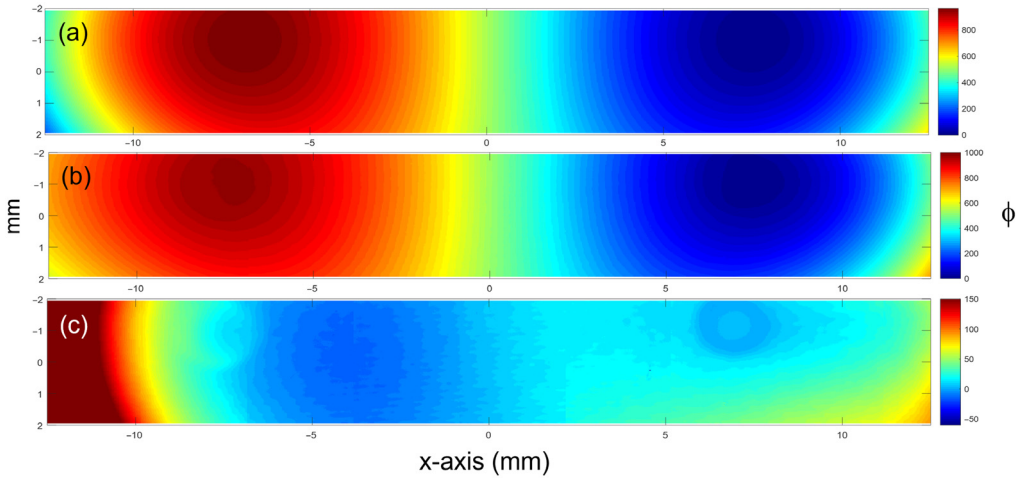

Fig. 10 Two-dimensional phase diagrams over a 4-mm height swath across center of device, constructed from (a) the cubic refractive index profile of design H, (b) compensated DHM measurements over same area, and (c) the difference between the "as designed" and compensated "as printed" designs. The residual aberrations at the edges are outside the clear aperture. Note the different phase scales for each plot.

Using DHM metrology, the wavefront information is digitally recorded as a hologram, from which the OPDs can be created using a numerical reconstruction algorithm. This allows for the printed refractive index profiles to be reconstructed. The deviation of the DHM-measured refractive index profiles from the design's refractive index profiles were used to confirm that the "as printed" parts meet the "as-designed" intent.

Figure 10(a) shows the phase delays from a 4-mm tall portion of the refractive index profiles from the GRIN Alvarez-Lohmann lens, Design H. Figure 10(b) shows the DHM measured phase delays, which have a linear tilt removed from the measured phase delays. Figure 10(c) shows the difference between the "as designed" parts and the compensated "as printed" parts. The phase profile of the DHM-measured parts showed a good overall match to the design intent. While there are residual errors at the edges of the device, the error is located at the border of the device, outside of the clear aperture of the lenses. Inside the eyebox there is residual WFE.

The optical power of the lens pair was tested over a range of lateral shift values, $+/-\delta$, by measuring the focal lengths as a function of the shift of the conjugate phase plates. Pictures of the eyebox, imaging underlying graph paper, are shown in Fig. 11, as a function of lateral shift. Shown in Fig. 12 are the optical powers, calculated from measured focal lengths, plotted as a function of lateral shift. A -4.7 to $+4.2$ range of diopter adjustment was measured over the $+/-7.5-$ mm range of translation specified for this application. While the measured diopter as a function of lens shift ($f/\Delta\delta$) was linear over most of the range of motion, there was a slight deviation from linearity at the positive limit of the optical power range (maximum $+\delta$).

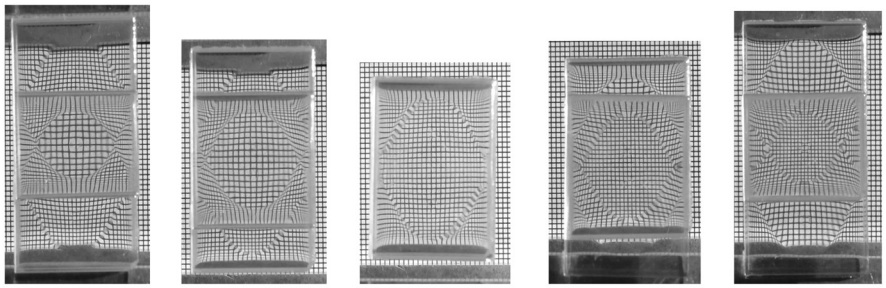

Fig. 11 Photograph of an Alvarez-Lohmann type lens pair imaging underlying grid, showing positive and negative change in optical power as a function of lateral shift distance and direction.

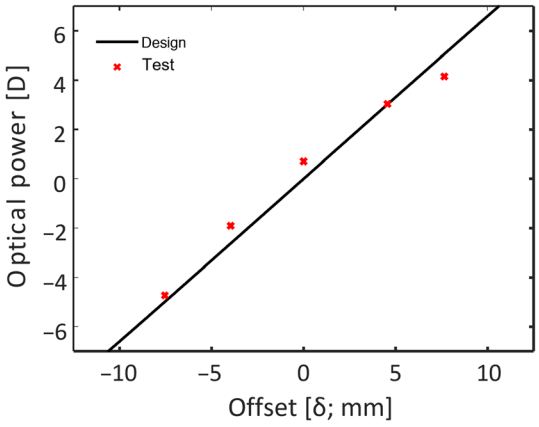

Fig. 12 Measured optical power (in diopters; D) as a function of lateral shift between the Alvarez-Lohmann type lens elements, compared to the linear design intent.

Analysis of the DHM measurements allowed us to identify that the $f/\Delta x$ nonlinearity was attributed to an unexpected tilt in the thickness of the elements. The wedge shape introduced to the design by equipment error introduced a slight optical prism, which could be easily simulated by treatment of the DHM measurements, as is shown in Fig. 10. The unintended optical prism prevented the lens pair to perform over the full diopter range of the design, although it was within the user-specified diopter adjustment range.

The thickness variation was attributable to a maladjusted screw, whose position is intended to maintain the print platform level while printing. With the deviation reproducible in simulations, and the source of the equipment error found, no attempt was made to polish or refabricate the lenses. The analysis proves the utility of DHM as a metrology tool for diagnostics and process control.

With this insight, the residual errors of Fig. 10(c) are likely to be due to non-linear effects resulting from tilt bias, which were not compensated. This hypothesis is supported by the location of the largest values of WFE errors at areas of large refractive index change, or transition regions such as at the apex. The large deviations outside of the clear aperture, at the far-left side of the residual phase plot Fig. 10(c), are "phase wrapping" artifacts, and may be ignored.

The halftoning algorithms may be refined to better accommodate these ranges of refractive index transition. Alternatively, measurements such as these can be used to compensate the print maps. These optimization methods are not dissimilar from optimizing mold designs or for compensating for tool paths when fabricating homogenous optics.

8.2 *Environmental Testing*

To prove robustness, the optics, integrated in the inserts, were environmentally tested using a 2-hr cycle with water immersion and detergent spray (up to 80°C) and functionality was demonstrated with a commercially available anti-fog coating. Specified six-foot drop tests onto concrete were also completed. Other printed optics were tested to MIL-STD-810G specifications including seven 24-hr temperature cycles from $+40$°C/100% relative humidity to -30°C/0% relative humidity, UV-exposure, and temperature shock tests. There we not measured changes in the focal length, as a function of lateral shift.

9 Conclusion

Gradient refractive index representations of an Alvarez-Lohmann lens were developed and used to fabricate and characterize the first reported variable optical power GRIN Alvarez-Lohmann lenses. These are also the first measured results from the more general category of freeform GRIN optics, and the first results reported for freeform GRIN optics fabricated using inkjet print additive manufacturing.

While an Alvarez- Lohmann configuration was shown herein, this approach may be generally extended to a wide range of refractive optical devices, consisting of two parts which, when translated with respect to each other, either laterally or rotationally, tune the optical properties of the device.[72] Furthermore, the problem of vision accommodation in respiratory masks is similar to that faced in AR and VR systems.

Due to the manufacturing constraints and the long fabrication times, GRIN optics has historically been limited to small diameter optics with mostly radially symmetrical gradient profiles of modest complexity. The demonstration of multiple 30 mm by 20-mm Alvarez-Lohmann lenses shows the practical utility of additive manufacturing for fabricating complex non-axisymmetric and freeform GRIN optical elements for specific applications. The benefit of inkjet print additive manufacturing is that freeform optical elements can be fabricated, on demand, directly from computer-aided design files, with minimal lead times and without the cost of custom tooling.

Unlike the surfaced homogeneously composed Alvarez-Lohmann lenses, GRIN Alvarez-Lohmann lenses may be plane parallel. The range of optical powers is limited only by the Δn. The work showed the advantages of optimizing the tilt terms of the GRIN Alvarez-Lohmann equation to maximizing the optical power, with minimal displacement, in the thinnest configuration. These design tradeoffs, not readily achieved in molded or diamond-turned surfaced Alvarez-Lohmann lenses, allowed for superb wavefront quality to be achieved.

Optimizing the design using optical feedstock with a larger Δn, will allow for a decrease in the lens thickness, or an increase in the diopter adjustment range. The larger Δn will also facilitate implementation of higher order polynomial terms for further aberration reduction, which was not implemented in this effort.

Further longitudinal optimization of the GRIN polynomial functions, in the direction of the optical axis, may also be used to improve performance over a wide gaze angle and to compensate for axis offsets. To minimize any constant aberrations, static compensating freeform GRIN elements may also be added to the design.

The GRIN Alvarez-Lohmann lenses were shown to satisfy an unmet need for vision accommodation in respiratory masks, which was not met using conventional optical technologies.

The ability to print the lens frame and the mechanical translation guide, along with fiducials and alignment marks, at the same time each lens element is printed, in a monolithic assembly, will allow for fine optical tolerances to be achieved, reducing post-fabrication alignment and assembly costs.

The ability to design freeform GRIN elements, along with their mechanical mounts, optimized for fabrication process parameters, with performance verified using metrology that reflects process control measures, demonstrates the utility and maturity of the additive manufacturing process for fabricating freeform GRIN optics.

Acknowledgments

The authors acknowledge the contributions to this work by Dr. Donald Conkey who performed the optical modeling and simulation. This work was funded by the U.S. Army Combat Capabilities Development Command Chemical Biological Center (DEVCOM) (Grant No. W911SR-17-C-0034). The authors declare no conflicts of interest.

References

1. D. H. Lippman et al., "Freeform gradient-index media: a new frontier in freeform optics," *Opt. Express* **29**, 36997–37012 (2021)
2. T. Yang et al., "Efficient representation of freeform gradient-index profiles for non-rotationally symmetric optical design," *Opt. Express* **28**, 14788–14806 (2020)
3. J. P. Rolland et al., "Freeform optics for imaging," *Optica* **8**, 161–176 (2021).
4. D. H. Lippman and R. Schmidt, "Prescribed irradiance distributions with freeform gradient-index optics," *Opt. Express* **28**, 29132–29147 (2020).
5. E. R. Dowski, Jr. and W. T. Cathey, "Extended depth of field through wave-front coding," *Appl. Opt.* **34**, 1859–1866, (1995).

6. L. W. Alvarez, "Two-element variable-power spherical lens," U.S. Patent No. 3,305,294 (1967).
7. L. W. Alvarez, "Development of variable-focus lenses and a new refractor," *J. Am. Optometr. Assoc.* **49**, 24–29 (1978).
8. A. W. Lohmann, "A new class of varifocal lenses," *Appl. Opt.* **9**, 1669–1671 (1970).
9. G. L. van Der Heijde, "Universal spectacles for children in developing countries," in *Proc. Mopane: Conf. Vis. Opt.* (2006).
10. S. Barbero, "The Alvarez and Lohmann refractive lenses revisited," *Opt. Express* **17**, 9376–9390 (2009).
11. I. A. Palusinski, J. M. Sasian, and J. E. Greivenkamp, "Lateral shift variable aberration generators," *Appl. Opt.* **38**, 86–90 (1999).
12. A. N. Simonov, G. Vdovin, and M. C. Rombach, "Cubic optical elements for an accommodative intraocular lens," *Opt. Express* **14**, 7757–7775 (2006).
13. C. Huang, L. Li, and A. Y. Yi, "Design and fabrication of a micro-Alvarez lens array with a variable focal length," *Microsyst. Technol.* **15**(4), 559–563 (2009).
14. A. C. Urness et al., "Arbitrary GRIN component fabrication in optically driven diffusive photopolymers," *Opt. Express* **23**, 264–273 (2015).
15. S. Ji et al., "Polymeric nanolayered gradient refractive index lenses: technology review and introduction of spherical gradient refractive index ball lenses," *Opt. Eng.* **52**(11) 112105 (2013).
16. J. Teichman et al., *Gradient Index Optics at DARPA*, Institute For Defense Analyses, Alexandria VA (2013).
17. E. W. Marchand, "Aberrations of wood and GRIN rod lenses," *Appl. Opt.* **25**(19), 3413–3417 (1986).
18. K. A. Richardson et al., "Advances in infrared gradient refractive index (GRIN) materials: a review," *Opt. Eng.* **59**(11), 112602 (2020).
19. T. Yang, *Freeform Gradient-Index Optics with Applications in Rotationally Variant Systems*, 29062821, University of Rochester ProQuest Dissertations Publishing (2022).
20. F. H. Long et al., "Generation and propagation of airy beams and one inch diameter focusing optics using 3D printed optics," *Proc. SPIE* **12135**, 1213507 (2022).
21. S. Maruca et al., "Generation and propagation of Airy beams and one inch diameter focusing optics using 3D printed polymer optics," *Proc. SPIE* **12103**, 1210306 (2022).
22. G. R. Schmidt, *Compound Optical Arrays and Polymer Tapered Gradient Index Lenses*, University of Rochester (2009).
23. J. N. Mait et al., "Chromatic analysis and design of a first-order radial GRIN lens," *Opt. Express* **23**, 22069–22086 (2015).
24. A. M. Boyd, "Optical design of multi-material, general rotationally symmetric GRIN lenses," *Proc. SPIE* **10998**, 109980J (2019).
25. D. Conkey, *Compressive 3D Imaging Spectrometer. No. DOE-VOXT-18800-1*, Voxtel, Inc. (2019).
26. J. P. Bowen et al., "Radial gradient-index eyepiece design," *Appl. Opt.* **27**(15), 3170–3176 (1988).
27. S. P. Wu, E. Nihei, and Y. Koike, "Large radial graded-index polymer," *Appl. Opt.* **35**(1), 28–32 (1996).
28. A. Visconti, "Design and fabrication of large diameter gradient-index lenses for dual-band visible to short-wave infrared imaging applications," PhD thesis, University of Rochester (2015).
29. J. Corsetti, "Design of ZnS/ZnSe gradient-index lenses in the mid-wave infrared and design, fabrication, and thermal metrology of polymer radial gradient-index lenses" PhD thesis, University of Rochester (2017).
30. G. M. Williams and J. P. Harmon, "Dispersion controlled nanocomposite gradient index lenses," *Opt. Contin.* **2**(2), 456–472 (2023).
31. G. M. Williams et al., "Additive manufacturing of freeform optics for defense applications," in *IEEE Res. and Appl. of Photonics in Defense* (2021).
32. S. D. Campbell et al., "Three-dimensional gradient-index optics via inkjet aided additive manufacturing techniques," in *IEEE Int. Symp. Antennas and Propag. & USNC/URSI Natl. Radio Sci. Meeting*, IEEE, pp. 605–606 (2015).

33. R. Dylla-Spears et al., "3D printed gradient index glass optics," *Sci. Adv.* **6**(47), eabc7429 (2020).
34. C. R. Ocier et al., "Direct laser writing of volumetric gradient index lenses and waveguides," *Light: Sci. Appl.* **9**(1), 196 (2020).
35. L. Yulin et al., "Research on micro-optical lenses fabrication technology," *Optik* **118**(8), 395–401 (2007).
36. A. Heinrich and M. Rank, *3D Printing of Optics*, SPIE Press, Bellingham, Washington (2018).
37. D. Zhang, X. Liu, and J. Qiu, "3D printing of glass by additive manufacturing techniques: a review," *Frontiers of Optoelectron.* **14**, 263–277 (2021).
38. Y. Zhu et al., "Recent advancements and applications in 3D printing of functional optics," *Addit. Manuf.* **52**, 102682 (2022).
39. J. W. Goodman, *Introduction to Fourier Optics*, McGraw-Hill, San Francisco (1968).
40. L. W. Alvarez and W. E. Humphrey, "Variable power lens and system," US Patent 3,507,565 (1970).
41. P. J. Smilie et al., "Design and characterization of an infrared alvarez lens," *Opt. Eng.* **51**(1), 013006 (2012).
42. S. S. Rege, T. S. Tkaczyk, and M. R. Descour, "Application of the Alvarez-Humphrey concept to the design of a miniaturized scanning 589 microscope," *Opt. Express* **12**, 2574–2588 (2004).
43. R. E. Stevens et al., "A review of adjustable lenses for head mounted displays," *Proc. SPIE* **10335**, 103350Q (2017).
44. J. Babington, "Alvarez lens systems: theory and applications," *Proc. SPIE* **9626**, 962615 (2015).
45. R. L. Truby and J. A. Lewis, "Printing soft matter in three dimensions," *Nature* **540**(7633), 371–378 (2016).
46. M. Singh et al., "Inkjet printing—process and its applications," *Adv. Mater.* **22**(6), 673–685 (2010).
47. Y. F. Liu et al., "Control of droplet formation by operating waveform for inks with various viscosities in piezoelectric inkjet printing," *Appl. Phys. A* **111**(2), 509–516 (2013).
48. W. Heller, "Remarks on refractive index mixture rules," *J. Phys. Chem.* **69**(4), 1123–1129 (1965).
49. J. N. Mait et al., "Dispersion design in gradient index elements using ternary blends," *Opt. Express* **24**(25), 29295–29301 (2016)
50. A. X. Desai, G. R. Schmidt, and D. T. Moore, "Achromatization of multi-material gradient-index singlets," *Opt. Express* **30**(22), 40306–40314 (2022).
51. R. R. Shannon, *The Art and Science of Optical Design*, Cambridge University Press (1997).
52. W. Besenmatter and C. Zeiss, "How many glass types a lensdesigner really needs?," in *Int. Opt. Design Conf.*, p. LTuC-2 (1998).
53. P.W. McCarthy, "Gradient-index materials, design, and metrology for broadband imaging systems," PhD thesis, University of Rochester (2015).
54. A. Visconti and J. L. Bentley, "Design of radial gradient-index lenses for dual-band visible to short-wave infrared imaging systems," *Opt. Eng.* **52**(11), 112106 (2013).
55. N. Mait et al., "Dispersion design in gradient index elements using ternary blends," *Opt. Express* **24**, 29295–29301 (2016).
56. G. Beadie et al., "Materials figure of merit for achromatic gradient index (GRIN) optics," *Proc. SPIE* **9822**, 98220Q (2016).
57. M. R. Bockstaller and E. L. Thomas, "Optical properties of polymer-based photonic nanocomposite materials," *J. Phys. Chem. B* **107**(37), 10017–10024 (2003).
58. Y. Imai et al., "Transparent poly (bisphenol A carbonate)-based nanocomposites with high refractive index nanoparticles," *Eur. Polym. J.* **45**(3), 630–638 (2009).
59. W. S. Kim, Y. C. Jeong, and J. K. Park, "Nanoparticle-induced refractive index modulation of organic-inorganic hybrid photopolymer," *Opt. Express* **14**(20), 8967–8973 (2006).
60. J. F. Jarvis, C. N. Judice, and W. H. Ninke, "A survey of techniques for the display of continuous tone pictures on bilevel displays," *Comput. Graphics Image Process.* **5**(1), 13–40 (1976).

61. Final report AFRL-RY-WP-TR-2016-0159, "Manufacturable Gradient Index Optics (M-GRIN) (2016).
62. B. Bourdoncle, J.-P. Chauveau, and J.-L. Mercier, "Traps in displaying optical performances of a progressive- addition lens," *Appl. Opt.* **31**, 3586–3593 (1992).
63. F. Wyrowski and J. Turunen, "Wave-optical engineering," in *International Trends in Applied Optics*, A. H. Guenther, Ed., SPIE Press, Bellingham, Washington (2002).
64. A. Moehl et al., "Ready to use a multi-focal system based on Alvarez lenses," *Proc. SPIE* **10690**, 1069017 (2018).
65. A. Wilson and H. Hua, "Design and demonstration of a vari-focal optical see-through head-mounted display using freeform Alvarez lenses," *Opt. Express* **27**, 15627–15637 (2019).
66. I. M. Barton et al., "Diffractive Alvarez lens," *Opt. Lett.* **25**, 1–3 (2000).
67. Williams, "Multi printhead refractive gradient inkjet printing," U.S. Patent US9855752B2, U.S. Patent and Trademark Office, Washington, DC (2016).
68. A. Zapata and S. Barbero, "Mechanical design of a power-adjustable spectacle lens frame," *J. Biomed. Opt.* **16**(5), 055001 (2011).
69. F. C. W. B. van Asbeck, "Combined lens and spectacles provided with at least one such combined lens," U.S. Patent No. 7,980,690, U.S. Patent and Trademark Office, Washington, DC (2011).
70. B. Spivey, "Adjustable focus eyeglasses," U.S. Patent No. 7,325,922, U.S. Patent and Trademark Office, Washington, DC (2008).
71. N. A. Dodgson et al., "Variation and extrema of human interpupillary distance," *Proc. SPIE* **5291**, 36–46 (2004).
72. S. F. Busch et al., "Extending the Alvarez-lens concept to arbitrary optical devices: tunable gratings, lenses, and spiral phase plates," *IEEE Trans. Terahertz Sci. Technol.* **7**(3), 320–325 (2017).

George M. Williams is the founder and president of NanoVox LLC. His work focusses on expanding the capabilities of modern optical and electro-magnetic enabled products, using additive manufacturing of engineered nanocomposite materials to expand the degrees of design freedom. He is a member of SPIE.

John Paul Harmen is vice-president research and development at NanoVox. He leads the research and development of inkjet print writing systems and print-optimized optical and RF nanocomposite feedstock. He is principal investigator on several U.S. Government Research Contracts. His previous background at Hewlett Packard includes significant contributions to the development and commercialization of inkjet printhead, inks, and printers.